MODIFICATION OF NEAR-WALL STRUCTURE IN A THREE-DIMENSIONAL TURBULENT BOUNDARY LAYER

Robert O. Kiesow and Michael W. Plesniak
School of Mechanical Engineering
Maurice J. Zucrow Laboratories
(formerly Thermal Sciences and Propulsion Center)
Purdue University
West Lafayette, IN 47907, USA

ABSTRACT

The near-wall physics and turbulence structure of a planar, shear-driven, three-dimensional turbulent boundary layer (3DTBL) are examined in a specialized facility with varying strengths of crossflow. The spanwise shear results in a modification of the near-wall turbulence structure. Analysis of flow visualization data reveals a reduction of mean streak length by as much as 50% with increasing spanwise shear, while streak spacing remains relatively constant. Power spectra of velocity confirm this shift towards higher temporal frequencies, corresponding to decreased streamwise length scales. Particle image velocimetry measurements indicate a significant modification of the inner region of the boundary layer with increasing spanwise shear. Streamwise velocity profiles exhibit an increasing velocity deficit with increased crossflow. Increased levels of the normal Reynolds stresses $\overline{u^2}$ and $\overline{v^2}$ and an increase in the $-\overline{uv}$ Reynolds shear stress are also observed. Notable modifications in the spanwise vorticity were also observed at higher shear rates.

INTRODUCTION

Most high Reynolds number flows of engineering interest are three-dimensional in nature and their extra rates of strain result in complex flow fields that are not fully understood (see reviews by Johnston and Flack, 1996; Eaton, 1995; Ölçmen and Simpson, 1992). Key features include non-colateral shear stress and strain rate vectors and decreasing ratio of the shear stresses to the turbulent kinetic energy with increasing three-dimensionality. These are indicators that the skewing has a significant effect on the structure of turbulence. A common feature of previous shear-driven experiments (e.g. Driver and Johnston, 1990) is their complex geometry and multiple strain rates. Computational studies (Moin et al., 1990; Sendstad and Moin 1992) have used direct numerical simulation (DNS) to examine planar channel flows subject to transverse pressure gradient. A more recent study by Coleman et al. (1996) includes both spanwise shear and transverse pressure gradient effects on a plane channel flow. These computational studies, along with pressure-driven and shear-driven experimental investigations, have contributed to the understanding of 3DTBLs.

Discrepancies, however, still exist in the literature concerning near-wall turbulence structure indicating a continued need for experimental and computational studies to expand the understanding of 3DTBLs and their associated turbulence structure. The objective of the current study is to investigate a planar, shear-driven 3DTBL having a simple geometry and also variation in the strength of the crossflow. The effects of crossflow are thus isolated from the confounding effects of streamwise pressure gradient, allowing closer examination of the near-wall structural features of the 3DTBL. Examination of the separate effects of skewing and streamwise pressure gradient is possible in this apparatus to complement numerical studies, e.g. the DNS of Coleman et al. (1996). This investigation is performed using flow visualization and particle image velocimetry (PIV) as well as using hot-film anemometry to evaluate the power spectra of the streamwise velocity.

EXPERIMENTAL APPARATUS AND TECHNIQUES

The planar, shear-driven 3DTBL is studied in a low-speed recirculating water tunnel specifically designed for this purpose. This facility provides a flat and smooth test surface along which a canonical 2-D boundary layer develops and is subsequently subjected to spanwise shear to generate a 3-D boundary layer. The Reynolds number, based on the momentum thickness, at the measurement location is Re_θ = 1450, and the boundary layer thickness is δ = 50 mm. A schematic of the 3-D turbulent boundary layer test plate is shown in Figure 1. This test plate supports an enclosed belt mechanism integrated into a section of the side wall to

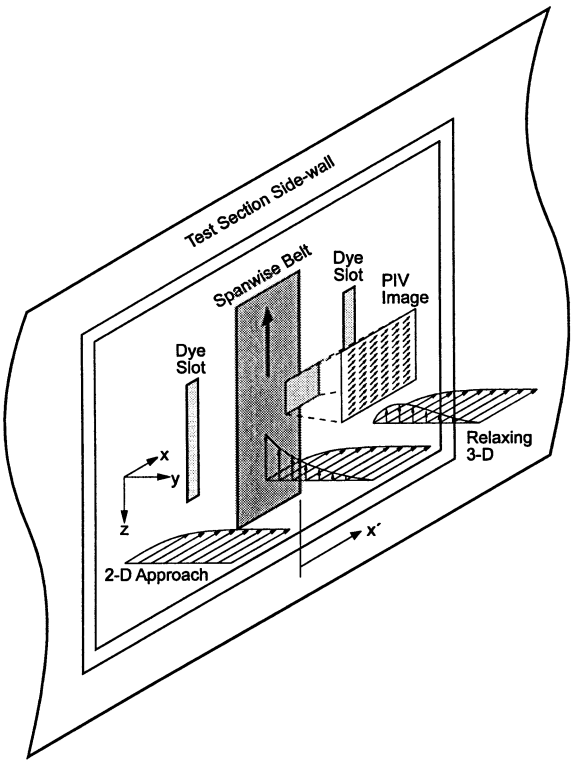

Figure 1. Schematic of 3-D turbulent boundary layer test plate.

provide a spanwise-translating motion, with variable speed capability. The shearing device is an enclosed transverse-translating belt mechanism embedded in the wall with a 12.7 cm wide by 38.1 cm high section of the belt exposed in the plane of the test section side wall. This corresponds to 50% of the span of the test section height and approximately two and a half boundary layer thickness in the streamwise direction. The shear-generating mechanism was operated at belt velocity ratios W_r = 0, 1.0, 2.0 and 2.75, i.e. the spanwise belt speed divided by the freestream velocity of the boundary layer, U_∞ = 27 cm/s.

Flow visualization using direct dye injection was performed to examine the structural features of the shear-driven boundary layer. The dye was introduced into the flow by means of two 20.3 cm long dye slots located approximately one and a half boundary layer thicknesses upstream and downstream of the translating wall, respectively. The dye solution consisted of fluorescein disodium salt dissolved in water at a concentration of 4 ppm. A laser light sheet, formed using a Coherent I-90 5W Argon-Ion cw laser and sheet-forming optics, was oriented in the *xz*-plane at y = 0.5 mm and y = 1.5 mm and was used to illuminate the fluorescent dye in the near-wall region.

Hot-film anemometry measurements were used to obtain the power spectral density of the streamwise velocity over a range of belt operating conditions. A DANTEC model R01 hot-film probe was used in conjunction with a TSI IFA-300 constant temperature anemometry system. The hot-film probe was positioned along the spanwise centerline approximately 1.5 δ downstream of the trailing edge of the translating belt. Measurements were acquired at a sampling rate of 20 Hz and filtered at 10 Hz to obtain spectra over a 10 Hz range at a resolution of 0.005 Hz. A sampling rate of 200 Hz and filtering at 100 Hz was also used to examine a larger frequency range at a resolution of 0.05 Hz.

Additionally, a DANTEC FlowMap PIV 2100 processor was used to obtain instantaneous measurements of two components of velocity in the *xy*-plane (side view) and *xz*-plane (plan view). The optical system consists of a NewWave 100mJ Nd:YAG laser with software-driven controls for the pulse separation time. Resolution of particle movement was found to be optimal with a pulse separation time of Δt = 0.9 ms. The laser beam propagates through sheet-forming optics to form a sheet that is approximately 1 mm thick and 150 mm wide. A Kodak® MEGAplus ES 1.0 CCD cross-correlation camera with a 1008(H) x 1018(V) pixel array provides on-line imaging capability. Controlled image acquisition, storage and display, and processing of the image to obtain the velocity data are accomplished on a personal computer running FlowManager software. The flow was seeded with 5 micron silicon carbide particles at a concentration of approximately 20 particles per mm^3. Typically, thirty images were ensemble-averaged to provide the mean flow velocities that were subtracted from an instantaneous flow image to reveal secondary flow patterns. In addition, up to 250 images were ensemble-averaged to obtain statistics for the mean flow velocity, rms velocities and Reynolds stresses.

Velocity vectors were determined from interrogation regions having a size of 0.84 mm x 0.84 mm. The overall uncertainty in the velocity measurements can be determined at a 95% confidence level following the methods of Moffat (1988). The uncertainty in the U and V velocities is estimated at ± 3% of the local measurement. Uncertainties in the Reynolds normal stresses $\overline{u^2}$ and $\overline{v^2}$ are estimated to be ± 9% of the local value. The uncertainty in the primary Reynolds shear stress, $-\overline{uv}$, is estimated to be on the order of ± 30% of the local measurement. This is a consequence of the limited ensemble size of 250 images used to estimate statistical quantities such as second order moments.

RESULTS

Laser-induced fluorescence (LIF) flow visualization studies were performed to investigate the flow structure in the near-wall region of the 3DTBL. The dye was introduced into the flow through the downstream dye slot located approximately one and a half boundary layer thickness downstream of the translating belt. The illuminating light sheet was positioned parallel to the wall at wall-normal locations of approximately *y* = 0.5 mm ($y^+ \approx 6$) and *y* = 1.5 mm ($y^+ \approx 18$) and allowed a 150 mm streamwise x 200 mm spanwise section of the near-wall region to be visualized with the fluorescent dye. Photographs of the LIF flow visualization at y = 0.5 mm revealed a modification of the near-wall streak structure due to the crossflow as reported in Kiesow and Plesniak (1997, 1998). The crossflow results in a reduction in the streak length by as much as 50% at higher shear rates compared to the 2-D base with no spanwise shear. However, there does not appear to be any significant

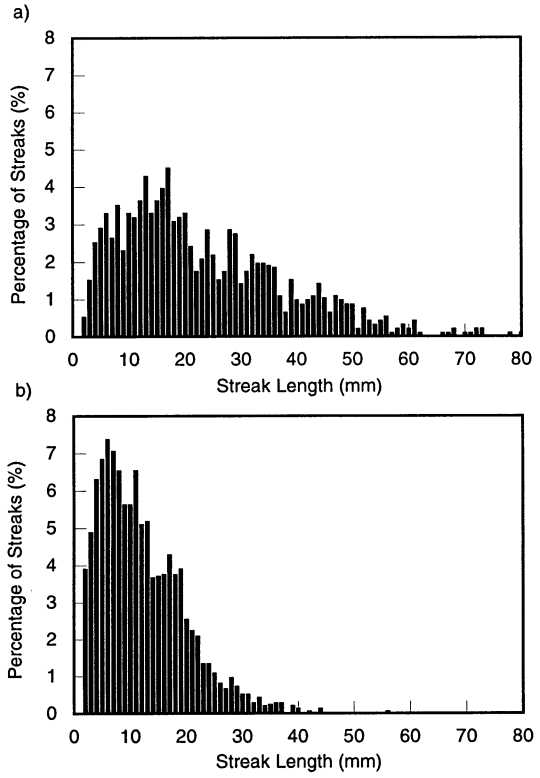

Figure 2. Histograms of streak length for a) $W_r = 0$ and b) $W_r = 2.0$.

modification of the streak spanwise spacing.

In order to quantify the observations of the LIF flow visualization, LIF images were digitized and with image enhancement, the wall streaks were identified, counted, and measured. Although this procedure entailed a certain amount of subjectivity in identifying streaks and determining their beginning and ends, the procedure was applied consistently to all of the images. Therefore, the resulting trends represent a reasonable picture of modifications to the streak structure. The image analysis resulted in sample sizes of approximately 900 streaks for the $W_r = 0$ case and 1300 streaks for the $W_r = 2.0$ case. The resulting histograms for the streak length for the base case and at a velocity ratio of 2.0 are shown in Figure 2. These histograms clearly show a shift towards smaller streamwise length scales with increasing spanwise shear and a narrower distribution of streak sizes compared to the 2-D base case. Both histograms are asymmetric; however, the $W_r = 2.0$ case exhibits a slightly higher skewness and kurtosis compared to the base case. Smaller standard deviations for the sheared cases, along with the reduction in mean streak length, are strong indications of a reduction in the streamwise length scales of the wall streaks in the near-wall region. These results are consistent with the DNS results of Sendstad and Moin (1992) as well as more recent results reported by Le et al. (1998) of a DNS and LES of a 3DTBL generated by a spanwise-moving wall in a channel.

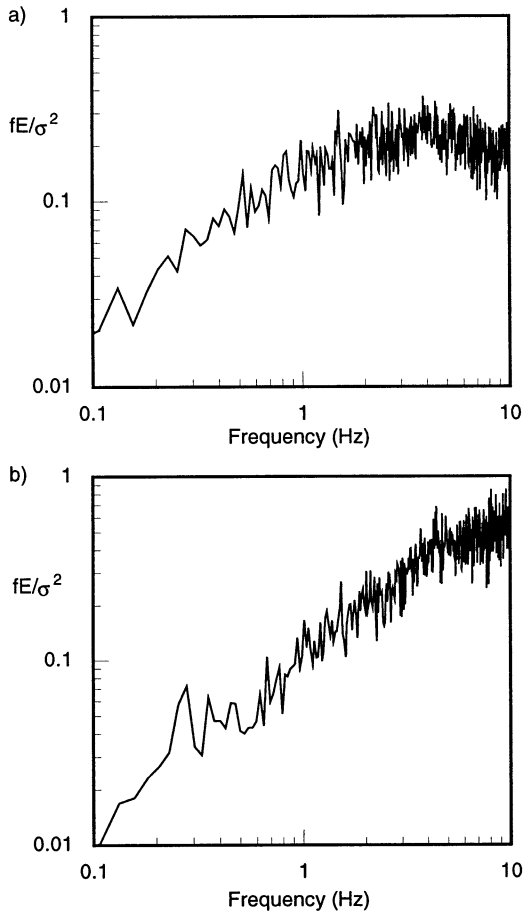

Figure 3. Non-dimensionalized power spectra at 1.5 δ downstream of belt edge at y = 6 mm for a) $W_r = 0$ and b) $W_r = 2.75$.

Plots of the one-dimensional normalized power spectra over a frequency range of 0 to 10 Hz for the 2-D base case and for $W_r = 2.0$ are shown in Figure 3. In these plots the power spectral density is premultiplied by the frequency and divided by the variance, so that the peak is centered about the most energetic frequencies. The effect of increasing spanwise shear is to shift the energy peak towards higher temporal frequencies, or smaller streamwise scales. For the 2-D base case, the most energetic frequencies are centered at 4 Hz. In contrast, for the $W_r = 2.0$ case, the peak energy has not only shifted to around 10 Hz (confirmed by spectra over the extended frequency range of 0 to 100 Hz not shown here), but the boundary layer has also become more energetic at these flow scales. Based on the aforementioned spectra and the two other cases examined, i.e. $W_r = 1.0$ and 2.75 (not shown), the effect of increasing spanwise shear is to cause a progressive growth of the flow energy and to shift the peak energy to higher frequencies. This observation of more energy at the higher frequencies and corresponding smaller scales corroborates the observed shift towards

smaller streamwise length scales in the LIF flow visualization results.

Particle image velocimetry measurements were obtained in a plane that is parallel to the flow and perpendicular to the wall (*xy* - plane). Image analysis produced simultaneous measurements of U and V components of velocity at a maximum of 6972 points over a uniform grid in an image region approximately 54 mm square. Measurements were obtained with the belt stationary in order to establish the base case for the 2-D boundary layer and with the belt operating at velocity ratios of W_r = 1.0, 2.0 and 2.75. The image region was located approximately on the spanwise centerline at a streamwise location that extended from x′ = -20 mm upstream to x′ = 30 mm downstream of the translating wall reference (x′ = 0 at the trailing edge of the belt.) Profiles obtained by Spalart (1988) using DNS of a 2-D flat plate boundary layer are plotted with solid lines to provide a benchmark for the PIV profiles. Note that exact agreement is not expected because of the difference in freestream turbulence levels between the experiment and simulation.

Mean statistics were determined from an ensemble average of 250 vector maps with 3969 points in each image. Boundary layer profiles for the four operating conditions at a streamwise location of x′ = 25 mm, corresponding to approximately half a boundary layer thickness downstream of the belt, are shown in Figure 4. These profiles of the mean streamwise velocity develop an increasingly severe velocity deficit in the inner region of the boundary layer with increasing spanwise shear. This velocity deficit is not very pronounced for the W_r = 1.0 case with mild crossflow. However, for the higher shear rates of W_r = 2.0 and 2.75 the deceleration of the streamwise velocity is significant, with the deficit region extending out to a y/δ of approximately 0.4. In the outer region of the boundary layer (y/δ > 0.4) the profiles are similar and essentially collapse onto a common curve. A strong velocity deficit is still evident at the higher shear rates at subsequent downstream locations (Kiesow and Plesniak, 1999). However, the magnitude of the deceleration of the streamwise velocity begins to decrease, indicating a relaxation of the 3-D flow.

Profiles of the normal Reynolds stress $\overline{u^2}$ are shown in Figure 5 for W_r = 0, 1.0, 2.0, and 2.75 at a streamwise location of x′ = 25 mm. These profiles were obtained from the ensemble average of three columns of PIV velocity vectors to reduce the scatter i.e. spatially averaged over 1.7 mm, or 0.04 δ. For the 2-D base case, the peak in the $\overline{u^2}$ profile occurs near the wall, at approximately the same location as the benchmark, but with higher intensity. The effect of weak spanwise shear (W_r = 1.0) is an initial decrease in the magnitude of the $\overline{u^2}$ normal stress in the near-wall region compared to the 2-D case. However, the more highly sheared cases of W_r = 2.0 and 2.75 show an increase in $\overline{u^2}$ out to y/δ ≈ 0.4 with an associated shift in the peak value away from the wall with increased spanwise shear. For the most highly sheared case of W_r = 2.75 the peak has shifted out to y/δ ≈ 0.2. In the outer region of the boundary layer (y/δ > 0.4) the profiles are similar and collapse onto a common curve.

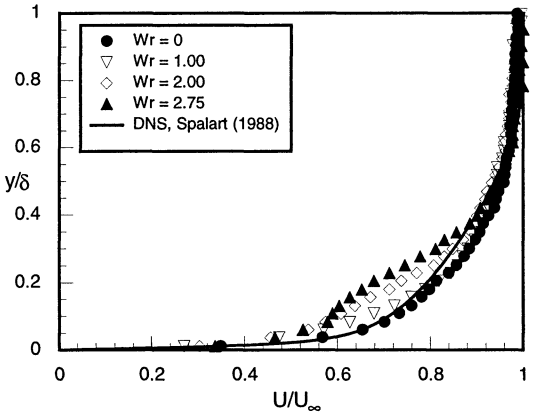

Figure 4. Boundary layer profiles of streamwise velocity at x' = 25 mm downstream of belt edge for velocity ratios of W_r = 0, 1.0, 2.0 and 2.75.

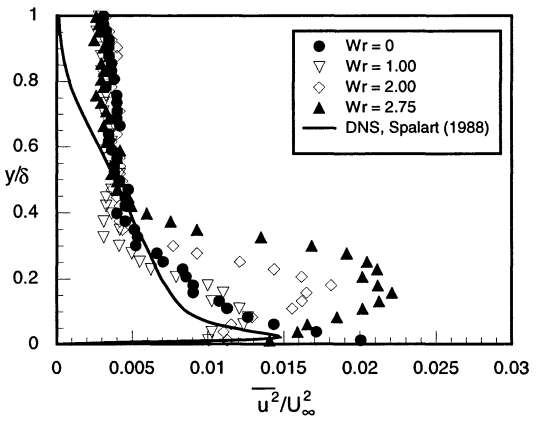

Figure 5. Profiles of $\overline{u^2}$ Reynolds stress at x' = 25 mm downstream of belt edge for velocity ratios of W_r = 0, 1.0, 2.0 and 2.75.

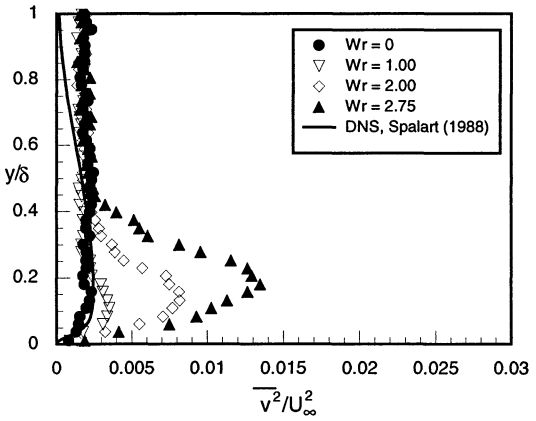

Figure 6. Profiles of $\overline{v^2}$ Reynolds stress at x' = 25 mm downstream of belt edge for velocity ratios of W_r = 0, 1.0, 2.0 and 2.75.

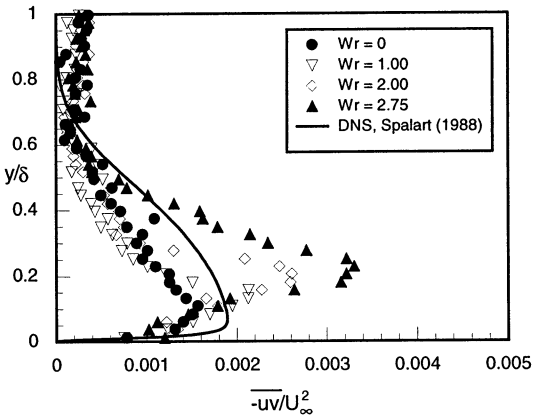

Figure 7. Profiles of $-\overline{uv}$ Reynolds stress at x' = 25 mm downstream of belt edge for velocity ratios of W_r = 0, 1.0, 2.0 and 2.75.

Corresponding profiles for the $\overline{v^2}$ normal Reynolds stress at x′ = 25 mm for all four belt velocity ratios are presented in Figure 6. The effect of increasing spanwise shear is a monotonic increase of the $\overline{v^2}$ normal stress away from the wall. For the most highly sheared case of W_r = 2.75 the magnitude of $\overline{v^2}$ is increased by almost an order of magnitude compared to the 2-D base case. A second effect of increased spanwise shear is to shift the peak in the $\overline{v^2}$ stress away from the wall. For the mildly sheared case of W_r = 1.0 the peak value occurs at $y/\delta \approx 0.1$ and for the most strongly sheared case of W_r = 2.75 the peak value has shifted out to $y/\delta \approx 0.2$. However, in the outer region of the boundary layer ($y/\delta > 0.4$) the profiles again collapse onto a common curve.

Profiles of the primary Reynolds shear stress $-\overline{uv}$ are shown in Figure 7 for W_r = 0, 1.0, 2.0, and 2.75 at a streamwise location of x′ = 25 mm. These profiles were also obtained from the ensemble average of three columns of PIV velocity vectors to reduce the scatter in the shear stress profiles. The effect of spanwise shear appears to be twofold. With increasing spanwise shear, the magnitude of the $-\overline{uv}$ Reynolds stress steadily increases below $y/\delta < 0.5$. For the most strongly sheared case of W_r = 2.75 the peak magnitude in $-\overline{uv}$ is increased by 130%. The second effect of the crossflow is to shift the peak in the $-\overline{uv}$ stress away from the wall with increased spanwise shear. For the 2-D base case, the peak in the $-\overline{uv}$ stress is located at $y/\delta \approx$ 0.10, while for the most highly sheared case of W_r = 2.75 the peak has shifted out to a $y/\delta \approx$ 0.25. Although three-dimensionality generally results in a reduction of the Reynolds stresses and a_1 parameter, the regions where the boundary layer is initially skewed exhibit an overshoot of $-\overline{uv}$. This trend has been reported in other studies e.g. Flack and Johnston (1994) and Compton and Eaton (1997). At subsequent downstream locations the peak in the $-\overline{uv}$ stress continues to shift further into the outer region of the boundary layer. However, the magnitude of the $-\overline{uv}$ stress begins to decrease, showing signs of a relaxing flow field

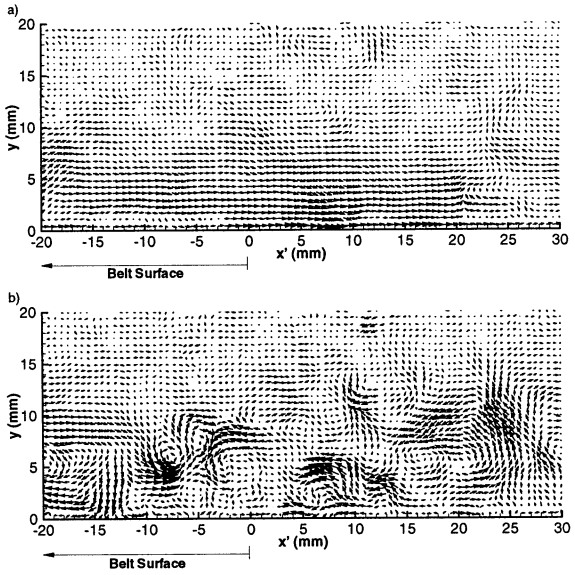

Figure 8. Secondary velocity fields in the *xy*-plane at belt trailing edge for velocity ratios a) W_r = 0 and b) W_r = 2.75.

(Kiesow and Plesniak, 1999).

Representative plots of the secondary flow fields for the 2-D base case of W_r = 0 and for the most strongly sheared case of W_r = 2.75 are shown in Figures 8. The secondary velocity field is obtained by subtracting the local mean velocity at each *y*-normal location in order to reveal secondary flow patterns. The secondary velocity field for W_r = 0 is fairly uniform with minimal variations in the magnitude of the secondary velocities and some regions of mild recirculation. In contrast, the secondary velocity field for the most strongly sheared case of W_r = 2.75 exhibits much larger variations in the secondary velocity magnitude. More frequent and significantly stronger regions of recirculation are also observed. These regions extend further into the outer region of the boundary layer (out to $y \approx$ 15 mm or $y/\delta \approx 0.3$) compared to the 2-D case.

Contour plots of the instantaneous spanwise vorticity, ω_z, for the aforementioned vector fields, are shown in Figure 9. The spanwise vorticity for the 2-D base case of W_r = 0 is concentrated in a layer of negative vorticity near the surface (y < 5 mm) where the velocity gradients are highest. The addition of spanwise shear results in a significant alteration of the ω_z distribution. With increased crossflow, the layer of spanwise vorticity along the surface is broken up and more isolated regions of both positive and negative extend further into the outer region of the boundary layer are present. For the most strongly sheared case of W_r = 2.75 numerous counter-rotating vortices of similar magnitude appear to exist. They are lifted off the surface and extend out into the boundary layer (out to $y \approx$ 15 mm or $y/\delta \approx 0.3$).

CONCLUSIONS

A specialized facility for generating a shear-driven 3DTBL allowed the near-wall turbulence structure to be examined for varying degrees of crossflow. LIF flow visualization reveals a modification of the near-wall streak

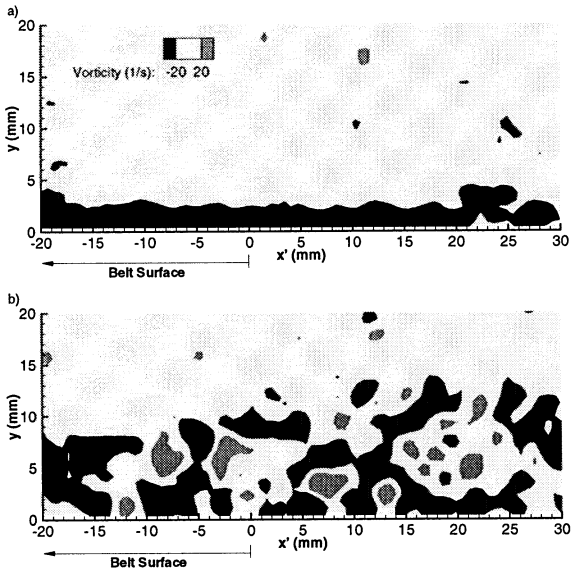

Figure 9. Contour plots of spanwise vorticity, ω_z, at belt trailing edge for velocity ratios a) $W_r = 0$ and b) $W_r = 2.75$.

structure when the turbulent boundary layer is subjected to spanwise shear. A reduction of mean streak length with increasing spanwise shear was measured, while streak spacing remained relatively constant. Histograms of streak length show a reduction of approximately 50% in mean streak length for a belt-to-freestream velocity ratio of W_r = 2.0. Power spectra of the streamwise velocity downstream of the belt confirm this shift towards smaller streamwise length scales, or higher frequencies. The addition of spanwise shear causes a shift of the inertial subrange and of the peak energy to higher frequencies, or smaller scales. PIV measurements in the *xy* - plane, at the trailing edge of the translating wall, indicate modifications of the inner region of the boundary layer due to the crossflow. Boundary layer profiles show a significant velocity deficit at $y/\delta < 0.4$ for the higher spanwise shear rates of W_r = 2.0 and 2.75. Profiles of turbulence quantities also show significant changes of the turbulence in the inner region of the boundary layer. Profiles of the normal Reynolds stresses indicate an increase in $\overline{u^2}$ and $\overline{v^2}$ with increasing spanwise shear out to $y/\delta < 0.4$. However, an initial decrease in $\overline{u^2}$ is observed in the near-wall region with increased crossflow. The $-\overline{uv}$ stress exhibits an overshoot of approximately 130% for the most highly sheared case of W_r = 2.75 and the peak in the $-\overline{uv}$ stress shifts away from the wall with increasing spanwise shear. Secondary velocity fields exhibit an increase in magnitude and stronger regions of recirculation with increasing spanwise shear. Another observed effect of the addition of crossflow is the breakup of the spanwise vorticity layer in the near-wall region compared to that in the 2-D base case. With increasing spanwise shear, the spanwise vorticity is distributed into smaller pockets of both positive and negative vorticity that extend throughout the inner region of the boundary layer. The overall effect of the crossflow in this planar, shear-driven 3DTBL is to disrupt near-wall coherent structures resulting in a shift to smaller length scales and an increase in the $\overline{u^2}$ and $\overline{v^2}$ normal Reynolds stresses and the $-\overline{uv}$ Reynolds shear stress in the inner region of the boundary layer.

REFERENCES

Coleman, G., Kim, J. and Le, A., 1996, "A numerical study of three-dimensional wall-bounded flows," *Intl. J. of Heat Fluid Flow* **17**, 333-342.

Compton, D., and Eaton, J., 1997 "Near-wall measurements in a three-dimensional turbulent boundary layer," *Journal of Fluids Mechanics* **350**, 189-208.

Driver, D., and Johnston, J., 1990, "Experimental study of a three-dimensional shear-driven turbulent boundary layer with streamwise adverse pressure gradient," *NASA Technical Memorandum* 102211.

Eaton, J., 1995, "Effects of mean flow three dimensionality on turbulent boundary-layer structure," *AIAA Journal* **33**, 2020-2025.

Flack, K., and Johnston, J., 1994, "Near-wall flow in a three-dimensional turbulent boundary layer on the endwall of a rectangular bend," *ASME Fluids Engineering Division* **184**, 1-19

Johnston, J., and Flack, K., 1996, "Advances in three-dimensional turbulent boundary layers with emphasis on the wall-layer regions," *Transactions of the ASME - Journal of Fluids Engineering*, **118**, 219-232.

Kiesow, R., and Plesniak, M., 1999, "Structural modifications and near-wall physics of a shear-driven 3-D turbulent boundary layer," *ASME FED Symp. on Complex and Separated Flows*, FEDSM99-7068.

Kiesow, R., and Plesniak, M., 1998, "Modification of near-wall turbulence structure in a shear-driven three-dimensional turbulent boundary layer," *Exp. in Fluids*, **25**, 233-242.

Kiesow, R., and Plesniak, M., 1997, "Near-wall physics and structure of a shear-driven 3-D turbulent boundary layer," *ASME FED Symp. on Complex and Separated Flows*, FEDSM97-3282.

Le, A., Kim, J., and Coleman, G., 1998 "A numerical study of turbulence modification in shear-driven 3DBL's," *51st DFD meeting of the American Physical Society, Philadelphia, PA.*

Moffat, R., 1988 "Describing the uncertainties in experimental results," *Experimental Thermal and Fluid Science* **1**, 3-17.

Ölçmen, M., and Simpson, R., 1992, "Perspective: On the near wall similarity of three-dimensional turbulent boundary layers," *Journal of Fluids Engineering* **114**, 487-495.

Sendstad, O., and Moin, P., 1992, "The near-wall mechanics of three-dimensional turbulent boundary layers," *Report* TF 57. Thermosciences Div. of Mech. Engng, Stanford University.

Spalart, P., 1988 "Direct simulation of a turbulent boundary layer up to R_θ = 1410," *Journal of Fluids Mechanics* **187**, 66-98.